

# Backgrounds and Detector Issues at a Muon Collider \*

S. Geer

*Fermi National Accelerator Laboratory, P.O. Box 500, Batavia, IL 60510*

## ABSTRACT

Backgrounds arising from muon decay at a 4 TeV muon collider are summarized, and some implications for a muon collider detector are discussed. Ideas on how to cope with the significant background levels are also described.

## I. INTRODUCTION

The physics case for a multi-TeV lepton collider has been extensively studied [1]. It is generally believed that new physics associated with electroweak symmetry breaking will manifest itself at or below the few TeV scale. If this new physics gives rise to new particles (e.g. SUSY, technicolor, extended gauge groups with new gauge bosons, ...) precise measurements of their properties will be essential to obtain a full understanding of the underlying physics. A lepton collider would seem to be the tool of choice for these precision measurements. A multi-TeV lepton collider will be needed if any of the new particles have masses close to 1 TeV or above, or if no new particles are discovered below 1 TeV in which case precise measurements of longitudinal WW scattering at high-energy are important. Hopefully we will begin to explore some of this new physics at TEV33, LEP2, and/or the LHC. However, it seems likely that our knowledge of any new physics beyond the Standard Model obtained at these machines will be incomplete, and that either a multi-TeV lepton collider or a very high energy hadron collider will become essential to move beyond the LHC energy scale. Unfortunately the performance of a multi-TeV  $e^+e^-$  collider is severely limited by beamstrahlung and (for circular machines) by synchrotron radiation. Furthermore, the two full energy linacs required for a linear  $e^+e^-$  collider may not be affordable. A possible solution is to build a muon collider. Since the muon is 207 times heavier than the electron, beamstrahlung is not a severe problem [2] and the drastic reduction in synchrotron radiation permits a circular collider. In addition, a multi-TeV muon collider would have the added bonuses that (i) the reduced beamstrahlung results in a reduced spread in center-of-mass energy yielding more precise energy scans, and (ii) for s-channel cross-sections that grow with mass squared (e.g. Higgs production) a muon collider has an advantage of  $(207)^2$  over an electron collider. If this was the whole story then the muon collider would be an obvious choice for a multi-TeV lepton collider. However, there are two major problems that must be overcome. First, more work is needed before it can be demonstrated that a muon collider will work (maybe it won't!). Second, muons decay giving rise to a large background flux through the detector. It has yet to be demonstrated that physics can be done in this background

environment (maybe it can't!). This second problem was considered in Refs. [3, 4], was subsequently the subject of a working sub-group [5] at Snowmass, and is the subject of this paper.

In the following we consider a 2+2 TeV muon collider with two bunches of  $2 \times 10^{12}$  muons per bunch, a luminosity of  $10^{35} \text{ cm}^{-2} \text{ s}^{-1}$ ,  $\beta^* = 3 \text{ mm}$ , and a beam-beam interaction region 3 mm long and  $3 \mu\text{m}$  radial rms. The time between bunch-bunch crossings is about 10  $\mu\text{s}$ . In Section II a summary of our current understanding of the background fluxes is presented. In Section III some general detector considerations are discussed. Sections IV and V discuss the background implications for vertex and outer tracking detectors, together with some ideas for trackers that have been discussed at Snowmass and are worthy of further consideration. Sections VI and VII discuss electromagnetic and hadronic calorimeter performance, and Section VIII discusses muon detection. Finally, a summary is given in Section IX.

## II. BACKGROUNDS

The main backgrounds at a muon collider are expected to come from the interactions of high energy electrons produced by muon decay. With  $2 \times 10^{12}$  muons per bunch and a beam energy of 2 TeV there will be  $2 \times 10^5$  muon decays per meter producing electrons with a mean energy of 700 GeV (see Fig. 1). These electrons are emitted at very small angles with respect to the beam direction, and hence stay within the beam-envelope until they see the magnetic fields of, for example, the final focus quadrupoles. On average, as the decay electrons traverse the fields of the final focus system they radiate 300 synchrotron photons with a mean energy of about 500 MeV, and therefore lose on average 20% of their energy before being swept out of the beam-pipe. The electrons can then interact in the beam-pipe walls, beam elements, or shielding to initiate electromagnetic showers. Important secondary interactions that contribute to the overall background flux are Bethe-Heitler muon pair production in the fields of the atomic nuclei ( $\gamma Z \rightarrow Z \mu^+ \mu^-$ ), muon pair production by electron-positron annihilation ( $e^+ e^- \rightarrow \mu^+ \mu^-$ ), and photonuclear interactions that result in a large flux of low energy protons and neutrons, and produce additional muons from hadron decay. The result of all these electron-induced interactions is a large flux of low energy electrons, photons, charged hadrons, and neutrons that are incident upon the detector volume together with a significant flux of higher energy prompt muons almost parallel to the beam directions. A careful design of the final focus system and the shielding immediately before the detector can reduce this background by several orders of magnitude [4]. Obtaining the optimal configuration is an iterative process which has not yet been completed. However, a factor of 100 reduction in the predicted background flux has already been

\* Work supported by the U.S. Dept. of Energy under contract DE-AC02-76CH03000

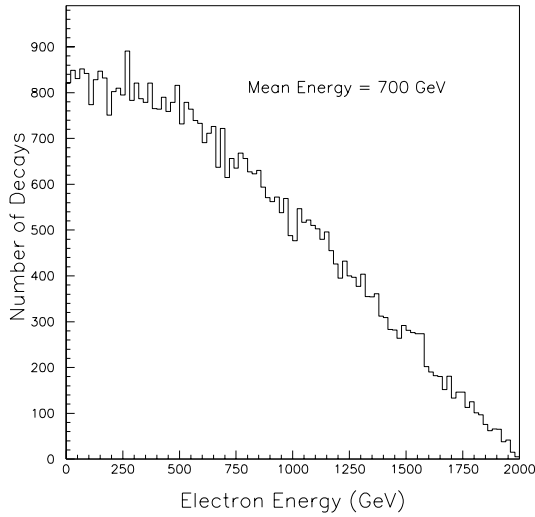


Figure 1: Energy distribution of electrons from 50000 simulated decays of 2 TeV muons. Courtesy of T. Diehl.

obtained. Furthermore, several further improvements to the lattice and shielding have been discussed at Snowmass and are expected to lead to an additional reduction of the predicted backgrounds.

The present background calculations, which provide a detailed simulation of all of the effects listed above, are described in Ref. [6] and summarized in the following sub-sections. Beam halo and beam-beam interactions will also contribute to the backgrounds seen by the detector. There will need to be a very efficient scraping system to eliminate beam halo on the far-side of the collider ring. This system has not yet been designed, and a model for the halo has not yet been developed. Hence beam-halo backgrounds are not included in the present calculations. The beam-beam interaction is also not yet in the background simulation. Eventually it will have to be included, however it is believed that backgrounds from this source will be relatively small [2].

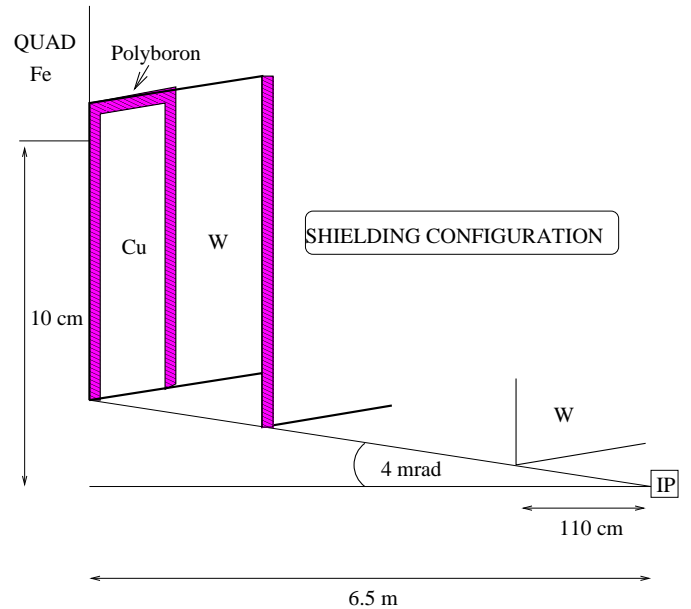


Figure 3: Shielding configuration implemented in the GEANT background calculation.

## A. Background Calculations

A correct understanding of the backgrounds is essential in order to develop a reasonable strawman detector design and understand the feasibility of doing physics at a muon collider. Two independent detailed background simulation programs have been developed. The first calculation has been developed by I. Stumer and is based on version 3.21 of the GEANT code used together with EGS [7] for electromagnetic shower simulation, FLUKA [8] to propagate hadronic showers, and MICAP [9] to transport low energy neutrons. The second calculation has been developed by N. Mokhov and is based on the MARS code [10]. These calculations have used different lattices, different shielding configurations, and different particle dependent energy cut-offs. In general the results from the two calculations are similar. Where there are significant differences, they can be understood in terms of the differences in the details implemented in the calculations. In the following the final focus and shielding configuration used in the GEANT calculation is described. The corresponding details for the MARS calculation can be found in Ref. [4].

The final focus geometry implemented in the GEANT calculation is shown in Fig. 2. The straight section before the interaction point (IP) is 130 m long, and consists of an 80 m long region containing no magnets followed by a 50 m long final focus region which accommodates the 4 final focus quadrupoles, 3 toroids, and an experimental hall containing the detector plus shielding. The toroids fulfill a double role; firstly they are scrapers for the electromagnetic debris, and secondly they sweep prompt muons away from the detector. The last 6.5 m before the IP is used for shielding to reduce the backgrounds in the detector volume as much as possible. The shielding occupies two cones that point at the IP with cone angles of  $20^\circ$ . The shielding

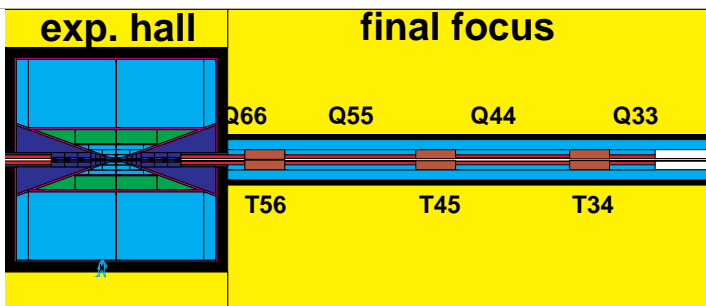


Figure 2: Region around the IP modelled in GEANT. The experimental hall and the final 50 m of the straight section immediately before the IP are shown.

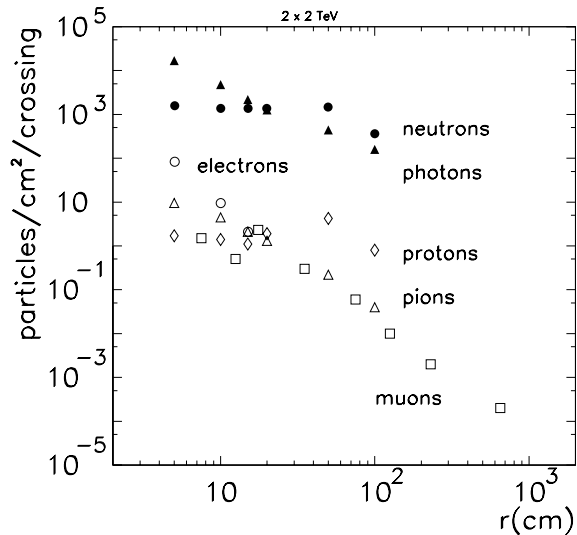


Figure 4: GEANT results: Radial particle fluxes shown as a function of radius in the detector volume. Calculation performed by I. Stumer.

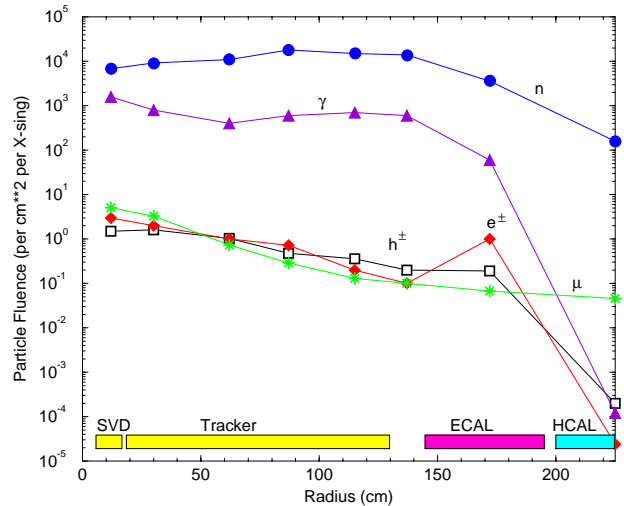


Figure 5: MARS results: Particle fluences (track length per unit volume) per bunch-bunch crossing shown as a function of radius in a  $\pm 1.2$  m central detector. Calculation performed by N. Mokhov.

geometry within these cones is shown in Fig. 3. The upstream end of each shielding cone has an entrance aperture of 2.5 cm, and can be thought of as a hadronic beam dump. It is constructed from copper absorber surrounded by a polyboron liner to reduce the neutron flux, and followed by a tungsten radiator to absorb electromagnetic showers. The inner surface of each piece of the dump is shaped like an inverted cone so that particles emitted from the surfaces cannot travel directly to the IP without passing through more material. The last part of the shielding, which has an inner aperture of 4.2 mm, is made of tungsten and can be thought of as an electromagnetic dump. Of the decay electrons that are produced throughout the 130 m long straight section, 2% interact in the last part of the shielding ("electromagnetic dump"), 30% interact in the "hadronic dump", 62% interact upstream of the shielding, and 10% pass through the interaction region without interacting. Finally, the "detector" implemented in the GEANT calculation consists of an evacuated tracking volume within a 2 Tesla solenoid field, surrounded by a copper-liquid argon calorimeter which starts at a radius of 150 cm and is 150 cm deep.

## B. Background Results

In the GEANT calculation electrons produced from muon decays occurring uniformly along the 130 m long straight section are tracked through the various magnetic fields of the quadrupoles, toroids, and detector solenoid. Showers induced by electrons and synchrotron photons interacting in the beampipe, magnets, and shielding are simulated down to particle cut-offs of 25 keV for electrons and photons, 0.00215 eV for neutrons, and 1 MeV for other hadrons. The GEANT code has been supplemented with a simulation of low energy photonu-

Table I: GEANT results: Longitudinal particle fluxes shown as a function of radius for photons, neutrons, electrons, pions, protons, and muons. The predicted fluxes (particles/cm<sup>2</sup>) correspond to the background from one bunch containing  $2 \times 10^{12}$  muons.

Radius (cm)	$\gamma$	n	$e^\pm$	$\pi^\pm$	p	$\mu^\pm$
Vertex						
5-10	7900	1100	69	14.4	0.8	1.5
10-15	3100	1200		3.7	0.05	0.5
15-20	1600	1000		4.6	4.0	2.3
Tracker						
20-50	450	870		0.8	3.9	0.3
50-100	120	520		0.1	2.2	0.06
100-150	130	330		0.003	0.4	0.01
160-310						0.002

clear interactions including the giant dipole, quasi-deuteron, meson, and quark fragmentation regions. The predicted fluxes of particles in the detector volume are shown as a function of radius in Fig. 4. The corresponding results from the MARS calculation are shown in Fig. 5. Despite the different lattices, shielding configurations, and energy cut-offs implemented in the two calculations, the MARS and GEANT predicted charged particle and photon fluxes are similar. The predicted neutron flux is a little higher in the MARS calculation, which is believed to reflect the presence of polyboron shielding surrounding the tracker volume in the GEANT simulation. The GEANT predicted longitudinal and radial particle fluxes are summarized in Tables I and

Table II: GEANT results: Radial particle fluxes shown as a function of radius for photons, neutrons, electrons, pions, protons, and muons. The predicted fluxes (particles/cm<sup>2</sup>) correspond to the background from one bunch containing  $2 \times 10^{12}$  muons.

Radius (cm)	$\gamma$	n	$e^\pm$	$\pi^\pm$	p	$\mu^\pm$
Vertex						
5	16900	1600	84.0	9.5	1.7	.35
10	4800	1400	9.4	4.5	1.4	0.43
15	2200	1400	2.1	2.1	1.1	0.33
20	1250	1400		1.3	1.9	0.20
Tracker						
50	440	1500		0.22	4.2	0.032
100	160	360		0.04	0.8	0.008

Table III: GEANT results: Mean energies of background particles in the tracking volume. The number in the rightmost column is for muons from pion decay only.

Particle	$\gamma$	p	$\pi^\pm$	n	$\mu^\pm$
$\langle$ Kinetic E $\rangle$ (MeV)	1	30	240	10	130

II respectively, and the mean particle energies are summarized in Tables III and IV. The predicted mean particle energies from the MARS calculation are summarized in Table V.

### C. Potential for Improvements

Several ways of improving the present lattice and shielding configurations have been discussed at Snowmass. In particular, the following modifications may lead to reductions in the predicted background fluxes:

- Additional dipoles: In the present lattice configuration there is an 80 m straight section before the final focus quadrupoles that is free. This straight section could accommodate additional dipoles to further suppress backgrounds originating upstream of the final quadrupoles.
- Dog Legs: The IP could be located above the machine plane by several meters if dog legs were implemented before the final focus quadrupoles. This might help to lower

Table IV: GEANT results: Mean energies of Bethe-Heitler muons passing through the detector volume.

Detector	Radius (cm)	Energy (GeV)
Vertex	10-20	24
Tracker	50-100	66
	100-150	31
Calorimeter	160-310	19

Table V: MARS results: Mean energies of background particles in the inner tracking volume [4]. The mean  $e^\pm$  energy includes a contribution from relatively high energy electrons trapped in the magnetic field, and is therefore higher than for the GEANT result. The mean  $\mu^\pm$  energy includes contributions from pion decay muons and from the higher energy muons, in contrast to the equivalent number in the GEANT table.

Particle	$\gamma$	$e^\pm$	$h^\pm$	n	$\mu^\pm$
$\langle$ E $\rangle$ , MeV	2.5	80	249	0.2	3630

the prompt muon flux through the detector and provide some protection against beam halo.

- Additional neutron shielding and moderation close to the tracking volume: reduction of the neutron flux has not yet been optimized. Additional neutron shielding and moderation might result in a reduced neutron flux.

This list is by no means complete. However, there are plans to try the three things listed above in the near future, and we can hope for at least a modest reduction in the predicted backgrounds.

## III. GENERAL DETECTOR CONSIDERATIONS

The predicted photon and neutron fluxes throughout the inner part of the detector volume are large. However, the mean photon and neutron energies are very low of the order of 1 MeV. Furthermore, at a given radius the longitudinal and radial fluxes of these particles are similar. Hence the dominant part of the background flux comes from a sea of very low energy neutral particles that do not come from the IP. We would expect this background sea to pepper the tracking volume with random hits, and produce significant energy pedestals in the calorimeter cells. These effects are considered in more detail in the following sections. In general, in designing a strawman detector that must operate in a large background flux we will want to employ as many detector channels as is practical. In Fig. 6 the number of non-pixel channels is shown for a random selection of large detectors as a function of the year when each detector first came into operation. It appears that the channel count increases by about an order of magnitude every 15 years. A strawman muon collider detector design with a few times  $10^6$  non-pixel channels would seem reasonable. Over the last few years pixel detectors have resulted in a revolution in "channel count". For example, the SLD vertex detector contains 300 million pixels, and similar numbers of pixels are planned for the LHC vertex detectors. Hence, a strawman muon collider vertex detector employing  $10^8$ - $10^9$  pixels would seem reasonable.

## IV. VERTEX DETECTOR CONSIDERATIONS

Consider the radial fluxes in the inner tracking volume. For example, at a radius of 10 cm there are 4800 photons/cm<sup>2</sup> with a

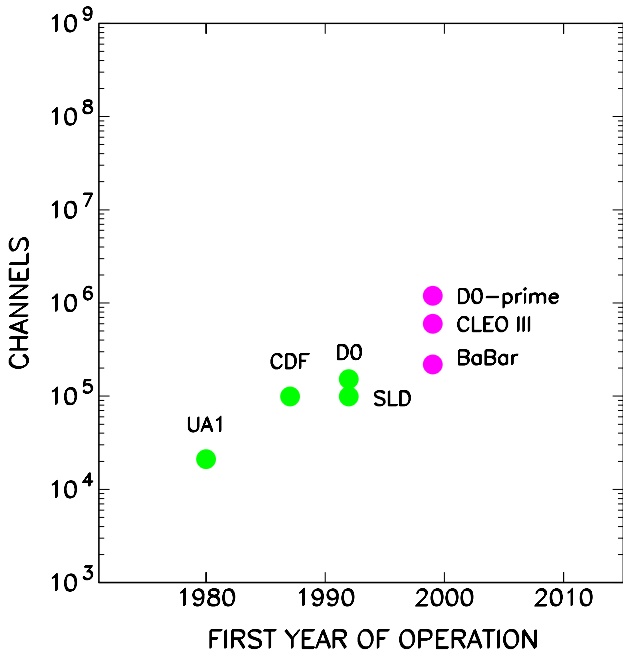


Figure 6: Number of non-pixel channels shown as a function of the first year of operation for a selection of detectors.

mean energy of 1 MeV, 1400 neutrons/cm<sup>2</sup> with a mean energy of 10 MeV, and 15.7 charged tracks per cm<sup>2</sup> which are mostly low energy electrons. Given these background fluxes we can estimate hit densities, occupancies, and radiation dose in a silicon pixel detector:

- Hit densities: To estimate the hit density in a silicon pixel layer we use interaction probabilities of 0.003 and 0.0003 for low energy photons and neutrons respectively. At a radius of 10 cm there are then 14.4 hits/cm<sup>2</sup> from low energy photon interactions, 0.42 hits/cm<sup>2</sup> from low energy neutron interactions, and 15.7 hits/cm<sup>2</sup> from charged tracks, yielding a total hit density of 31 hits/cm<sup>2</sup>. This hit density is comparable to the charged track density of about 40 hits/cm<sup>2</sup> observed in the inner layer of the SLD vertex detector, which works well. Hence, a priori the hit density in the vertex detector does not appear to be a problem if pixel technology can be used.
- Occupancies: To estimate occupancies we will assume a pixel size of  $50 \times 300 \mu\text{m}^2$ . The calculated occupancy is then 0.5%. If the vertex detector consists of 4 cylindrical 1 meter long layers at radii of 10 cm, 20 cm, 30 cm, and 40 cm then the total surface area to be covered is  $6.3 \times 10^4 \text{ cm}^2 \rightarrow 4.2 \times 10^8$  pixels. This example is not intended to be a strawman design. It does however suggest that sensible choices for pixel size and channel count yield calculated occupancies that do not appear to be a problem.
- Radiation dose: Of greater concern is the very large neutron flux which may severely limit the useful lifetime of a silicon detector in the tracking volume. The neutrons can be thought of as a gas with only a slow radial depen-

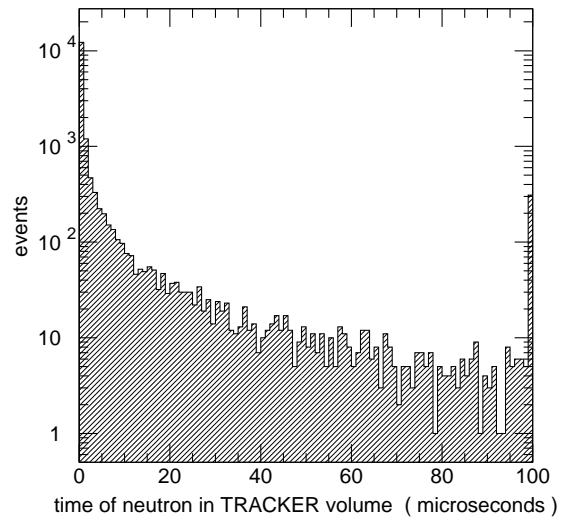


Figure 7: GEANT prediction for the time dependence of the neutron flux in the tracker volume. Calculated by I. Stumer.

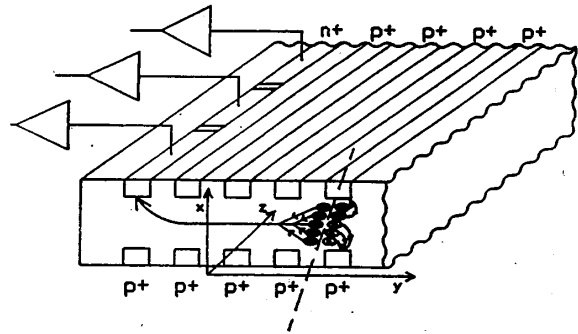


Figure 8: Silicon drift vertex detector.

dence. Fig. 7 shows the dependence of the neutron flux with time after the bunch-bunch crossing. The next crossing occurs after  $10 \mu\text{s}$ , by which time the neutron flux from the previous crossing has fallen by about 2 orders of magnitude, and can therefore be neglected. To a first approximation there are  $O(10^3)$  neutrons/cm<sup>2</sup> per crossing through the inner tracking volume. If muon bunches are injected into the collider at 15 Hz, and are used for 1000 orbits, then the resulting neutron flux in the inner tracker is  $O(10^7)$  neutrons/cm<sup>2</sup>/sec. This is comparable to the equivalent flux of neutrons at a radius of 10 cm through the CMS detector at the LHC operating at a luminosity of  $10^{34} \text{ cm}^{-2} \text{ s}^{-1}$  [4]. Although challenging, the CMS collaboration believe that silicon pixel detectors can be used in this environment [11].

These considerations suggest that the background rates may be low enough to permit the use of silicon pixel technology for

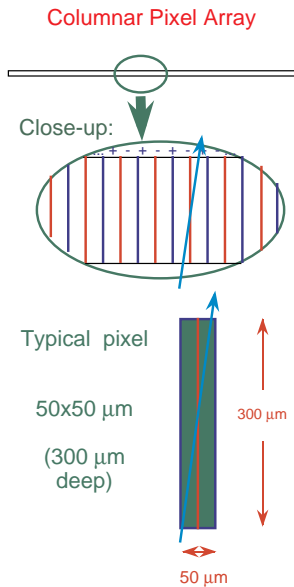


Figure 9: Columnar pixel geometry. Courtesy of A. Sill.

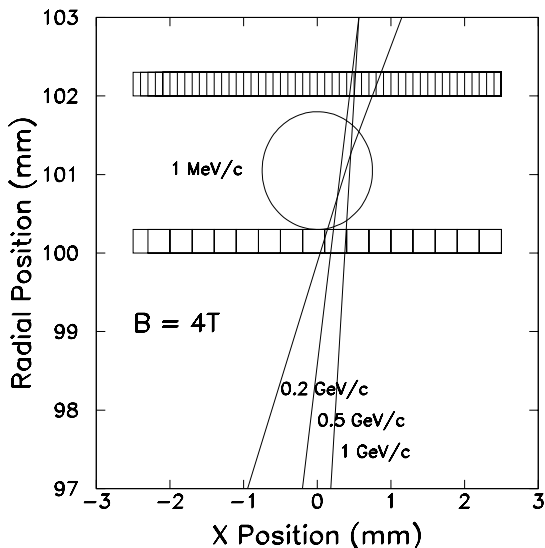


Figure 10: Pixel Micro-telescope geometry, showing trajectories of 0.2 GeV/c, 0.5 GeV/c, and 1 GeV/c tracks coming from the IP and bending in a 4 Tesla field.

the vertex detector. A good goal for further improvements in the lattice and shielding designs is to reduce the neutron flux in the tracking volume by a further order of magnitude. This would ease the concern that the lifetime of a silicon detector in the tracking volume is at best marginal. Assuming that silicon can be used for the vertex detector, several more explicit ideas about the vertex detector technology have been discussed at Snowmass:

- Silicon Drift Detector. The idea, which is described in the muon collider book [6], is to exploit the  $10 \mu\text{s}$  be-

tween bunch-bunch crossings by using the silicon drift detector technology developed by E. Gatti and P. Rehak [12] (Fig. 8). Using  $50 \times 300 \mu\text{m}^2$  detectors it should be possible to obtain a resolution of a few microns in the drift direction. This would facilitate a very precise vertex detector.

- Columnar Pixels, developed by S. Parker et al. [13] and proposed for use at a muon collider by A. Sill. The idea is to exploit the very well localized primary vertex position by using long thin tracking pixels that point at the IP and therefore record large ionization signals only for tracks coming from the IP (Fig. 9). For example, one can imagine  $50 \times 50 \mu\text{m}^2$  pixels that are  $300 \mu\text{m}$  deep. The pixels are produced using controlled feed-through-drilling technology to create a lattice of anodes and cathodes that extend through the  $300 \mu\text{m}$  thick wafer.
- Pixel Micro-Telescopes, proposed by S. Geer with read-out details developed by J. Chapman [14]. The idea is to replace a single pixel layer with two layers separated by a small distance, and read them out by taking the AND between appropriate pairs. The distance between the layers is optimized so that soft MeV tracks (which are associated with almost 80% of the predicted background hits) produced in one layer curl up in the magnetic field before reaching the second layer. Thus, the pixel micro-telescope is blind to the soft background hits and also blind to tracks that do not come from the IP. In the example shown in Fig. 10 the top measurement layer has a finer granularity than the bottom confirmation layer. The corresponding rows in the two pixel layers can be read out with different clock speeds to maintain the correct correspondence at the input into the AND gate that registers valid hits in the telescope. If the readout rows are the ones parallel to the beam direction, then variable clock speeds can be used to maintain the correct accepted direction with respect to the IP.

The challenge of a high background environment is clearly fruitful ground for new ideas. The above considerations suggest that, provided silicon detectors can be used in the inner tracking volume, it should be possible to construct a vertex detector able to tag b-jets etc at a muon collider. Detailed simulations are required to confirm this impression.

## V. OUTER TRACKER CONSIDERATIONS

Consider the radial fluxes in the outer tracking volume. The predicted background fluxes at a radius of 50 cm are  $440 \text{ photons/cm}^2$ ,  $1500 \text{ neutrons/cm}^2$ , and  $4.5 \text{ charged tracks per cm}^2$  which are mostly low energy protons. The neutron flux is therefore about the same as the flux in the inner tracking volume, whereas the photon and charged particle fluxes are significantly less than those predicted at smaller radii. There are two alternative tracking strategies to consider:

- Low field, large tracking volume drift chamber option. This option, which is described in the muon collider book [6], uses a TPC to exploit the  $10 \mu\text{s}$  time between bunch-bunch crossings. The large neutron flux necessitates choosing a gas that does not contain hydrogen. A

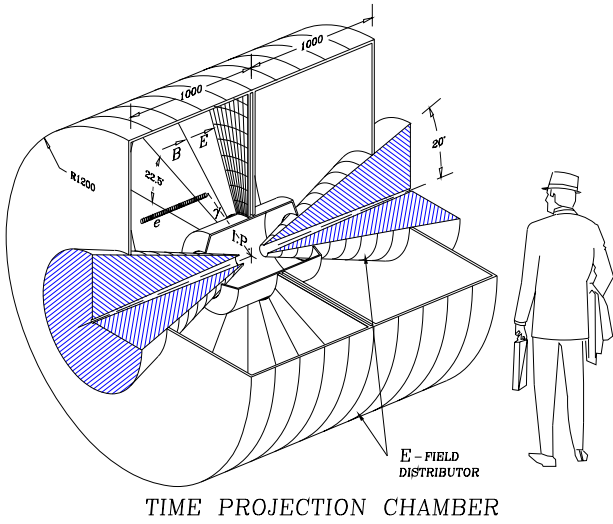


Figure 11: Outer tracker TPC.

mixture of 90% Neon plus 10%  $\text{CF}_4$  gives a drift velocity of  $9.4 \text{ cm}/\mu\text{s}$ , which is in the right ballpark. High- $p_T$  tracks from the IP imbedded in the predicted background flux have been simulated for the TPC shown in Fig. 11. The simulation includes ionization, drift and diffusion of the electrons in the gas, multiplication, and other details of the detection process. The majority of the background hits come from low energy Compton recoils yielding very

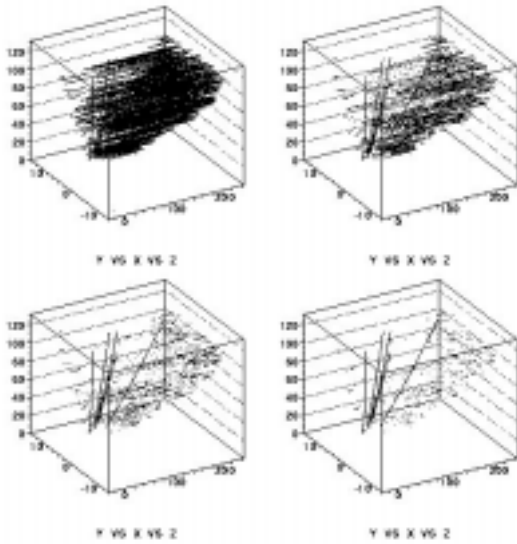


Figure 12: Simulated track hits in the outer tracker TPC for real tracks from the vertex imbedded in a sea of background hits from Compton scatters of low energy photons. The background is suppressed by rejecting large pulse heights. In the figures going from top-left  $\rightarrow$  bottom-right the hits are shown as the maximum pulse height accepted is reduced.

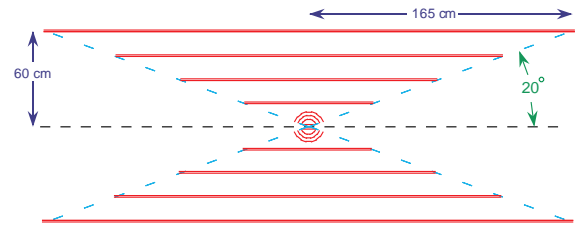


Figure 13: Compact tracker geometry in a 4 Tesla field.

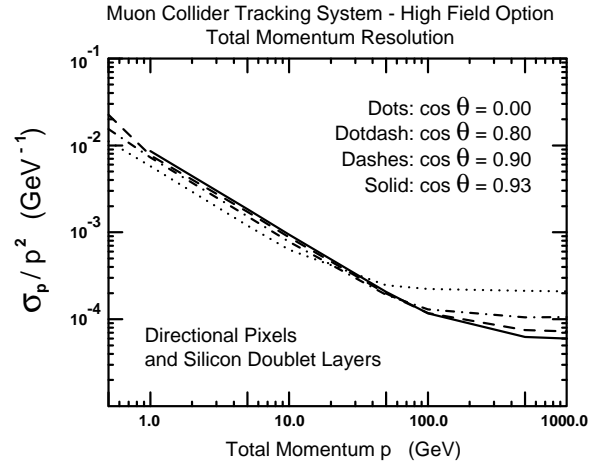


Figure 14: Compact tracker momentum resolution, calculated by A. Sill.

low energy electrons that have a radius of curvature of less than 1 mm in the 2 Tesla field, and their projection on the readout plane covers not more than one readout pitch ( $0.3 \times 0.4 \text{ cm}^2$ ). These background electrons, together with the nuclear recoils from neutron scatters, yield large pulses that can be removed by cutting on the maximum acceptable pulse height. The simulation predicts that with an average background flux of  $100 \text{ photons}/\text{cm}^2$ , reasonable pulse height cuts remove only 1% of the effective TPC volume, and yield the clean bubble chamber like tracks shown in Fig. 12. However, it was realized during the Snowmass discussions that positive ion build-up may be a problem with the design shown in Fig. 11. If this problem can be overcome, the design shown in the figure yields a simulated momentum resolution of about 1.2% for tracks with  $p_T = 50 \text{ GeV}/c$ .

- High field, compact silicon tracker option. An alternative strategy is to make a compact tracker by using silicon in a high field (for example, 4 Tesla). As an example, consider the geometry shown in Fig. 13 in which a 4-layer pixel vertex detector is imbedded in a 4-layer small angle stereo cylindrical silicon microstrip detector with a  $50 \times 300 \mu\text{m}^2$  resolution. Taking the inner layer of the vertex detector to consist of a cylinder of  $50 \times 300 \mu\text{m}^2$  pixels, and the outer 3

vertex layers to consist of spherical shells of  $50 \times 50 \mu\text{m}^2$  columnar pixels or pixel micro-telescopes. The system is assumed to correspond to 15% of a radiation length at  $90^\circ$ . Results are shown in Fig. 14 from a parametric calculation of the momentum resolution, which includes multiple scattering and yields  $\sigma_p/p^2 = 10^{-4} (10^{-2}) (\text{GeV}/c)^{-1}$  for  $p = 100 \text{ GeV}/c$  ( $1 \text{ GeV}/c$ ).

Both the low field and high field tracking solutions look interesting, and should be pursued with more complete simulations. Positive ion build-up may be a problem for the TPC solution, and radiation hardness may be a problem for the silicon solution. These potential problems need to be more fully understood.

## VI. ELECTROMAGNETIC CALORIMETER CONSIDERATIONS

Background particles entering the electromagnetic calorimeter are expected to give rise to significant energy pedestals in the calorimeter cells. Consider a 4 m long calorimeter that is 25 radiation lengths deep, has an inner radius of 120 cm, and is constructed from  $2 \times 2 \text{ cm}^2$  cells. There are then a total of  $7.5 \times 10^4$  electromagnetic calorimeter towers. The GEANT background calculation predicts that each cell sees on average  $n_\gamma = 400$  background photons per crossing with a mean energy  $E_\gamma = 1 \text{ MeV}$ . If an electromagnetic shower occupies 4 cells, then the mean background pedestal will be about 1.6 GeV. This pedestal can be subtracted from the measured energies. The precision of the resulting electron and photon energy measurements will depend on the fluctuations in the mean background energy per cell. This is estimated:

$$\sigma_{E_{CBLL}} = \sqrt{2n_\gamma} E_\gamma = 30 \text{ MeV} \quad (1)$$

which takes account of both the fluctuations in the numbers and mean energies of the photons incident on the calorimeter cells. For an electromagnetic shower occupying 4 cells, the fluctuations in the energy pedestals are therefore predicted to be about 60 MeV.

## VII. HADRONIC CALORIMETER CONSIDERATIONS

Consider a cylindrical hadronic calorimeter with an inner radius of 150 cm that is 2.5 m deep (about  $10 \lambda$ ), covering the polar angle range from  $30^\circ$  to  $150^\circ$ . The calorimeter is then about 10.5 m long. If the calorimeter is constructed from  $5 \times 5 \text{ cm}^2$  cells, there will be a total of about  $4 \times 10^4$  hadronic calorimeter towers. The GEANT background calculation predicts a mean energy deposition of about 1 GeV per tower per crossing. The fluctuations on this average pedestal are estimated to be:

$$\sigma_{E_{CBLL}} = \sqrt{2n_\gamma} E_\gamma = O(100 \text{ MeV}) \quad (2)$$

There is an additional source of concern for the hadronic calorimeter, namely the contribution from the prompt muons which pass through the calorimeter nearly parallel to the beam

directions and have a mean energy of 19 GeV. The GEANT calculation predicts a flux of  $0.002 \text{ muons}/\text{cm}^2$  per crossing, resulting in about 1000 muons per crossing passing through the hadronic calorimeter. These muons occasionally undergo nuclear interactions and deposit large amounts of energy in the calorimeter. An example of the predicted background energy deposited in the hadronic calorimeter is shown in Fig. 15 for the passage of a single muon bunch. The nuclear interactions result in background spikes in the towers with energies  $O(10) \text{ GeV}$ . A possible solution to this problem is to use fine longitudinal segmentation for the calorimeter towers so that hadronic showers initiated within the calorimeter and propagating parallel to the beam directions can be recognized and subtracted. This may mean that the longitudinal segmentation will need to be comparable to the transverse cell size, say 10 cm. In this extreme case there are 25 samples per tower, giving a total of about  $10^6$  hadronic calorimeter channels. This is probably feasible. However, a more modest longitudinal segmentation may be adequate. This clearly needs to be studied with detailed simulations, and the resulting missing transverse energy resolution for the calorimeter calculated.

## VIII. MUON DETECTOR CONSIDERATIONS

The predicted background flux is expected to be relatively modest at radii of greater than 3 m, in the vicinity of the muon detector. Several possible technologies for muon detectors at a muon collider were discussed during Snowmass:

- Cathode strip chambers. The idea, which is described in the muon collider book [6], is to use MWPCs with segmented cathodes and a short (35 ns) drift time to provide prompt signals for triggering. The precision of the co-ordinate

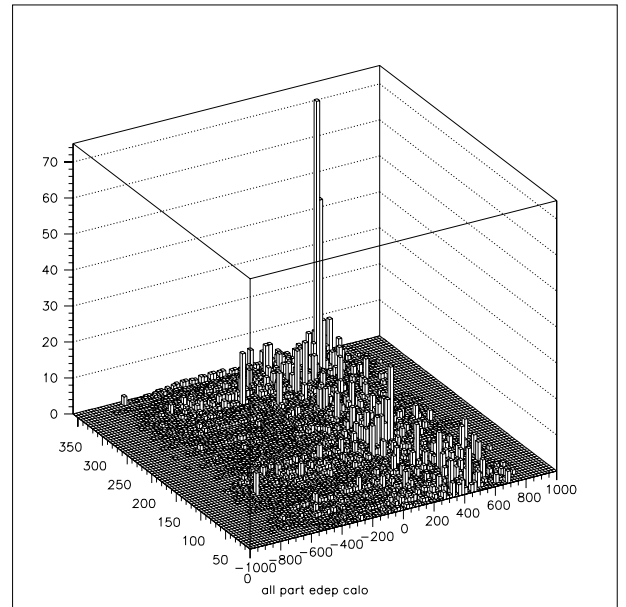


Figure 15: GEANT simulation of the energy deposited by Bethe-Heitler muons in the hadronic calorimeter for a single muon beam bunch.



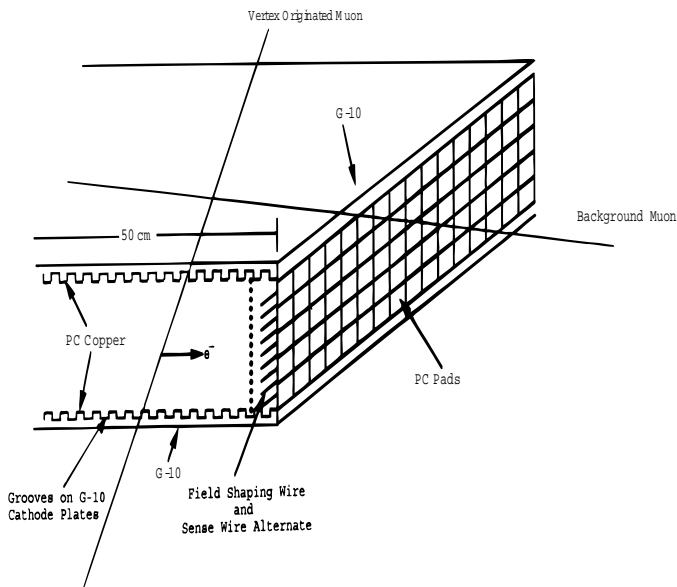


Figure 16: Long drift jet chamber with pad readout for muon detection at a muon collider. Courtesy of M. Atac.

measurement would be expected to be of order  $50 \mu\text{m} \times$  a few mm.

- Threshold cherenkov counter, proposed for the muon collider by D. Summers. The idea is to use a gas cherenkov radiator to exploit the directionality of cherenkov radiation in order to select high- $p_T$  muons coming from the IP. The device would also give excellent timing resolution (of order 2 ns).
- Long drift jet chamber with pad readout, proposed for the muon collider by M. Atac (Fig. 16). Drift time provides the Z co-ordinate, and pad readout provides the  $r$ - $\phi$  co-ordinates. Directionality at the trigger level is provided by the pattern of pad hits within a limited time window. The drift field is provided by cathode strips on grooved G-10 plates. Using 90% argon plus 10%  $\text{CF}_4$  and a maximum drift distance of 50 cm, the maximum drift time is  $5 \mu\text{s}$ .

## IX. SUMMARY

The background fluxes due to muon decay at a 4 TeV muon collider have been calculated using both GEANT-based and MARS-based simulations. The predicted background fluxes are sensitive to the lattice and shielding configurations, which have not yet been optimized. Although large, the predicted backgrounds are sufficiently close to being manageable with existing or foreseen detector technologies, that further work on optimization of the shielding and lattice is certainly justified. In particular, if the neutron flux can be reduced by about an order of magnitude, then it should be possible to use silicon technology for the vertexing and tracking. In this case, it appears that precision tracking and b-tagging will be achievable at a muon collider. The backgrounds entering the calorimeters are predicted to create substantial energy pedestals. More complete detector simu-

lations are needed to understand how the fluctuations on these pedestals affect the overall detector performance. In particular, prompt muons undergoing a nuclear interaction in the hadronic calorimeter create energy spikes that in principle can be recognized and removed if the longitudinal segmentation is sufficient. This needs to be demonstrated with a detailed simulation.

In conclusion, backgrounds from muon decay at a muon collider make the design of the detector, and its associated shielding, challenging. However, no show stoppers have been identified at Snowmass. Although substantial, the predicted backgrounds seem to be close to being "OK". Indeed, the predicted neutron and charged track fluxes through the tracking volume are not very different from those that will be experienced at the LHC [4] ! It should be noted that the discussion in this paper has been restricted to the central part of a muon collider detector. Perhaps the more challenging forward detectors will provide fruitful ground for new ideas.

## X. REFERENCES

- [1] See for example J. F. Gunion, *Physics Motivations for a Muon Collider*, UCD-96-16, May 1996.
- [2] I.J. Ginzburg, *The  $e^+e^-$  pair production at a  $\mu^+\mu^-$  collider*, hep-ph/9601273(1996); P. Chen, *Beam-Beam Interaction in Muon Colliders*, SLAC-PUB-7161(1996).
- [3] G.W. Foster and N.V. Mokhov, *Backgrounds and Detector Performance at a  $2 \times 2$  TeV  $\mu^+\mu^-$  Collider* AIP Conference Proc. 352 on Physics Potential and Development of  $\mu^+\mu^-$  Colliders, Sausalito, CA 1994, p. 178, FERMILAB-Conf-95/037. Proc. Symposium on Physics Potential and Development of  $\mu^+\mu^-$  Colliders, San Francisco, CA, Dec. 1995, FERMILAB-Conf-96/062.
- [4] N.V. Mokhov, *Comparison of Backgrounds in Detectors for LHC, NLC, and  $\mu^+\mu^-$  Colliders* Proc. Symposium on Physics Potential and Development of  $\mu^+\mu^-$  Colliders, San Francisco, CA, Dec. 1995, FERMILAB-Conf-96/062.
- [5] Muon Collider Detector and Background Working Group Participants: M. Atac, J. Brau, D. Burke, J. Chapman, P. Chen, G. Crawford, C. Damerell, T. Diehl, S. Geer, G. Gollin, H. Gordon, J. Gunion, B. Jacobsen, H. Jensen, C. Johnstone, S. Kahn, K. Kephart, P. Lebrun, D. Lissauer, T. Markiewicz, N. Mokhov, F. Paige, M. Peskin, R. Rehak, R. Roser, A. Sill, I. Stumer, D. Summers, A. Tollestrup, E. Willen.
- [6]  *$\mu^+\mu^-$  Collider: A Feasibility Study*, The  $\mu^+\mu^-$  Collider Collaboration, BNL-52503; Fermilab-Conf.-96/092; LBNL-38946 (1996).
- [7] R.L. Ford and W.R. Nelson, *The EGS Code System: Computer Programs for the Monte Carlo Simulation of Electromagnetic Cascade Showers*, SLAC-0210, 1978.
- [8] A. Fasso, A. Ferrari, J. Ranft, and P.R. Sala, *FLUKA: present status and future developments*, Proc. IV Int. Conf. on Calorimetry in High Energy Physics, La Biodola (Is. d'Elba), Italy, Sept. 1993.
- [9] C. Zeitnitz and T. Gabriel, Nucl. Instr. Meth., A349, 106(1994).
- [10] N.V. Mokhov, *The MARS Code System User's Guide, version 13(95)*, FNAL-FN-628(1995).
- [11] *CMS Technical Proposal*, The CMS Collaboration, CERN/LHCC 94-38 (1994).
- [12] E. Gatti and P. Rehak, Nucl. Instr. and Meth. 225, 608(1984).

- [13] Sherwood I. Parker, Christopher J. Kenney, Julie Segal, *3D: A New Architecture for Solid State Radiation Detectors*. UH-511-839-96, 24pp. Submitted to Nucl.Instrum. Methods.
- [14] S. Geer and J. Chapman, *The Pixel Micro-Telescope*, Contribution to these proceedings.